RCS Optimization Analysis Method for Sea-Skimming Unmanned Aerial Vehicle Based on Back Propagation Neural Network Algorithm

Chengpan Yang [1], Wei Yan [1,2*], Yang Zhao [1], Lu Geng [3], Shiliang Hou [1], and Jian Chen [1]

[1] School of Electrical and Automation Engineering
Nanjing Normal University, Nanjing, Jiangsu, 210097, China
61197@njnu.edu.cn

[2] Zhenjiang Institute for Innovation and Development
Nanjing Normal University, Zhenjiang 212004, China

[3] China Energy Engineering Group, Nanjing, Jiangsu, 211102, China

Abstract ─ The radar cross section (RCS) of sea-skimming unmanned aerial vehicle (UAV) can be influenced by the sea surface scattering under different sea conditions. In this paper, a composite model of the rough sea surface and sea-skimming UAV is established. A hybrid algorithm based on the application of physical optics (PO) method and improved multilevel fast multipole algorithm (PO-IMLFMA) for solving the RCS of the composite model based on four-path model (FPM) is proposed. Compared with multilevel fast multipole algorithm (IMLFMA) and PO and method of moment (PO-MOM), PO-IMLFMA has the advantages of less memory consumption (about 295 MB) and faster solution speed (about 768 s) for solving the composite model. Furthermore, in view of the influence of sea surface on the RCS of sea-skimming UAV, a compensation scheme based on back propagation (BP) neural network for the RCS of UAV is proposed. The compensation scheme is analyzed for the monostatic RCS of sea-skimming UAV under different sea conditions. The compensation results show that the compensation errors under 1-scale, 3-scale and 5-scale sea conditions are less than 0.95 dBsm, 0.41 dBsm and 1.94 dBsm, respectively. In other words, the compensation scheme significantly reduces the influence of sea conditions.

Index Terms ─ back propagation (BP) neural network, four-path model (FPM), improved multilevel fast multipole algorithm (IMLFMA), physical optics (PO), Radar cross section (RCS), sea conditions, unmanned aerial vehicle (UAV).

I. INTRODUCTION

With the rapid development of ocean construction in the world, sea-skimming aircraft has been widely used in quite a few aspects such as ocean reconnaissance and disaster prevention. The sea-skimming unmanned aerial vehicle (UAV) can fly over the sea at extremely low altitudes when they perform various tasks [1]. The scattering of sea-skimming UAV can be hidden through the help of scattering of sea surface. Radar cross section (RCS) can be used to quantitatively characterize the stealth performance of targets. The electromagnetic scattering characteristics of sea-skimming UAV and the influence of sea clutter on the scattering characteristics of sea-skimming UAV can be analyzed by the study of RCS. The study of composite electromagnetic scattering characteristics of rough sea surface and target is widely used in radar detection, marine remote sensing and military confrontation, and becomes an effective means to solve the problem of radar detection and tracking of sea objects [2]. The RCS of UAV usually varies randomly with time or radar incident angle in the course of flight.

In [3-4], the RCS problem of UAV was considered from different angles. The RCS of three-dimensional (3-D) electrically large object can be calculated by the finite-difference time-domain (FDTD) algorithm [5], method of moments (MOM) [6-7], the multilevel fast multipole algorithm (MLFMA) [8-9], physical optics (PO) and the Kirchhoff Approximation (KA) methods [10-12]. The RCS of the UAV can be calculated accurately by the above numerical algorithms, but the influence of actual environment such as the rough sea surface on the electromagnetic scattering characteristics of targets is not considered.

Common models of the rough sea surface are Pierson-Moskowitz (PM) spectrum [13], Elfouhaily spectrum [14], and Philips spectrum [15]. Rayleigh was one of the first people to propose a mathematical model of rough sea surface [16]. Pino used the Monte Carlo method to construct a one-dimensional sea surface model and analyzed the electromagnetic scattering

Submitted On: October 13, 2019
Accepted On: December 15, 2019

characteristics of two-dimensional (2-D) objects above the sea surface by the generalized forward and backward iteration method (GFBM) [17]. In [18], the inhomogeneous fast plane wave algorithm is used to study the composite RCS characteristics of 2-D rough surface and 3-D complex objects above it. However, the RCS of sea-skimming UAV considering the sea conditions is not studied by above methods, and the RCS compensation method for the object under the influence of sea surface is not proposed. In this paper, the RCS of the composite model of the sea-skimming UAV and the 2-D rough sea surface is established based on four-path model (FPM). Then, the RCS of the composite model is calculated and analyzed by the new hybrid numerical method based on the application of the PO method and improved multilevel fast multipole algorithm (IMLFMA).

The RCS value of rough sea surface will affect the RCS value of UAV when solving or measuring the RCS of sea-skimming UAV. In order to eliminate this unnecessary influence, a strong non-linear fitting algorithm - back propagation (BP) neural network algorithm is introduced in this paper [19-20]. The relationship between different incident angles, azimuth angles, RCS values of the rough sea surface, RCS values of composite model and RCS values of sea-skimming UAV is obtained by the nonlinear mapping of BP neural network.

The structure of this paper is organized as follows. A model of rough sea and sea-skimming UAV is established in Section II. In Section III, the RCS of the sea-skimming UAV considering the sea conditions is analyzed by the IMLFMA based on the FPM. A RCS compensation method based on BP neural network for sea-skimming UAV is presented in Section IV. Section V validates and analyzes the algorithm proposed in this paper. Finally, a conclusion is presented in Section VI.

II. MODELING FOR RCS CALCULATION OF ROUGH SEA SURFACE AND SEA-SKIMMING UAV

A. Rough sea surface modeling based on Monte Carlo method

The sea conditions studied in this paper are the sea surfaces under different wind and wave scales. The basic parameters of the international sea conditions standard are shown in Table 1. Where W. h. stands for the wave height, W. v. represents the wind velocity. The sea surface model is generally considered to be rough surface within the scope of electromagnetic scattering calculation. Rough surface has strong randomness and can be represented by relevant statistical parameters, including power spectral density, root mean square deviation, correlation function, root mean square slope, and radius of curvature.

Table 1: Parameters of international sea conditions standard

Scale	Name	W. h. (*m*)	W. v. (*m*/*s*)
1	Tiny wave	0 - 0.30	0 - 3.08
2	Middle wave	0.91 - 1.52	6.17 - 7.71
3	Billow	2.44 - 3.66	10.28 - 12.85

The power spectrum, known as the wave spectrum, is the most important statistical parameter in rough sea surface modeling. It reflects the distribution of harmonic components in azimuth and spatial frequency, and is the result of Fourier transform of sea surface height fluctuation correlation function. In this paper, the rough sea surface is modeled based on the PM spectrum under different wind speeds. The PM spectrum is:

$$S(\omega)=\alpha\frac{g^2}{\omega^5}\exp\left\{-\beta\left(\frac{g}{U\omega}\right)^{-4}\right\}, \quad (1)$$

where α=8.1×10^{-3} and β=0.74 are dimensionless empirical constants, g is the gravitational acceleration, g = 9.81 *m*/*s*$^{-2}$, U is the average wind speed at a height of 19.5 *m* above the sea surface and ω is angular frequency.

The randomly rough sea surface model under different sea conditions is simulated by Monte Carlo method. The main principle is to filter the power spectrum in the frequency domain and then the inverse fast Fourier transform is performed to obtain the discrete height values of the rough surface.

A two-dimensional rough sea surface of size $Dx \times Dy$ needs to generate $N \times M$ grids in the x and y directions with Δx and Δy as the steps. The height $z=f(x_n,y_m)$ of each point on the rough surface at $(x_n=n\Delta x,\ y_m=m\Delta y)$, ($n$ = -N/2 + 1,..., N/2; m = -M/2 + 1, ..., M/2) can be expressed as:

$$f(x_n,y_m)=\frac{1}{D_xD_y}\times \sum_{p=-\frac{N}{2}+1}^{\frac{N}{2}}\sum_{q=-\frac{M}{2}+1}^{\frac{M}{2}}F\left(k_{x,p},k_{y,q}\right)e^{-jk_{x,p}x_n}e^{-jk_{y,q}y_m}, \quad (2)$$

where F is a coefficient, given by,

$$F\left(k_{x,p},k_{y,q}\right)=2\pi\sqrt{D_xD_yW\left(k_{x,p},k_{y,q}\right)} \times\begin{cases}\dfrac{N(0,1)+iN(0,1)}{\sqrt{2}} & p=1,...,\dfrac{N}{2}-1;q=1,...,\dfrac{M}{2}-1\\ N(0,1) & p=0,\dfrac{N}{2};q=0,\dfrac{M}{2}\end{cases}, \quad (3)$$

where $k_{x,p}$ stands for the coefficient related to the x direction whereas $k_{y,q}$ is the coefficient related to the y direction. Specifically $k_{x,p}=2\pi p/D_x$, $k_{y,q}=2\pi q/D_y$.

In order to generate 2-D rough surfaces of real sequence, $F(k_{x,p},k_{y,q})$ must be conjugate symmetric with respect to the origin as shown in (4) and (5):

$$F\left(-k_{x,p},-k_{y,q}\right)=F^{*}\left(k_{x,p},k_{y,q}\right), \quad (4)$$

$$F\left(k_{x,p},-k_{y,q}\right)=F^{*}\left(-k_{x,p},k_{y,q}\right). \quad (5)$$

The PM spectrum is selected as the power spectrum and converted into polar coordinate form as:

$$W\left(k_{x,p},k_{y,q}\right)=W_1\left(K,\phi\right), \quad (6)$$

where $K=\sqrt{k_{x,p}^2+k_{x,q}^2}$, $\phi=\arctan\left(k_{y,q}/k_{x,p}\right)$.

The PM spectrum $W_1(K,\phi)$ can be solved by:

$$W_1\left(K,\phi\right)=\Phi(K,\phi)\frac{\overline{W}(K)}{K}, \quad (7)$$

$$\overline{W}\left(K\right)=\begin{cases}S(\omega)\sqrt{g/K}/2 & K>0\\ 0 & K<0\end{cases}, \quad (8)$$

where $S(\omega)$ ($\omega=\sqrt{gK}$) can be obtained by (1). If rough surface is approximately isotropic, $\Phi(K,\phi)=1/(2\pi)$.

According to (2), sea surface models under different wind speeds can be simulated. Referring to the Table 1, the sea surface models under 1-scale sea condition with 1 *m/s* wind speed, 3-scale sea condition with 7 *m/s* wind speed and 5-scale sea condition with 12 *m/s* wind speed are established respectively, as shown in Fig. 1.

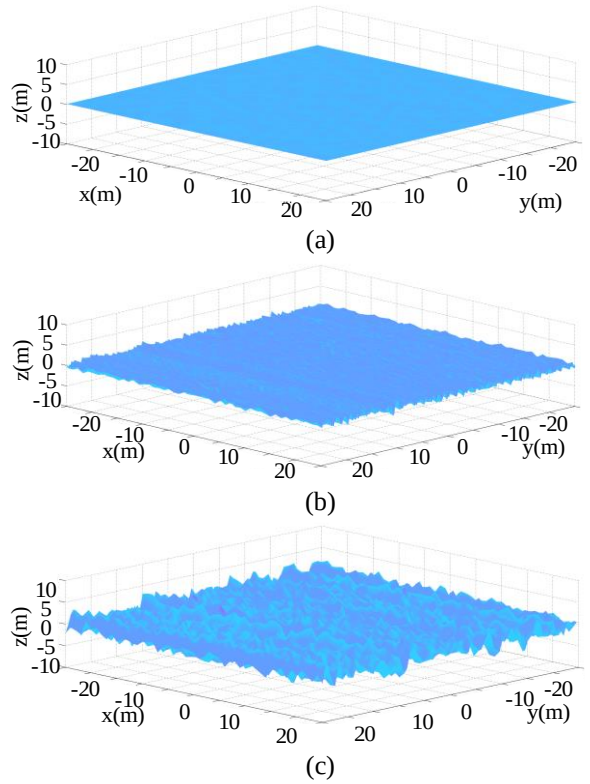

Fig. 1. Sea surface model under different sea conditions. (a) 1-scale Sea condition (wind speed 1*m/s*). (b) 3-scale sea condition (wind speed 7*m/s*). (c) 5-scale sea condition (wind speed 12 *m/s*).

B. Construction of RCS calculation model for sea-skimming UAV

The RCS calculation model of sea-skimming UAV is established especially for the electromagnetic scattering problem. The electromagnetic scattering characteristics of each component of UAV have some degree impact on the RCS of the entire aircraft. Therefore, the scattering contribution of components is also considered in the structural design of UAV besides aerodynamic requirements. Compared with strong scattering components, some details of UAV have little contribution to the total scattering field, which can be neglected. So the RCS calculation model of sea-skimming UAV focuses on the components with strong scattering contribution. The following components are considered in UAV modeling:

1) Wing and tail. The wing is modeled with a twist-free wing, so the front and rear edges of the wing are not considered. The parameters of the tail are similar to those of the wing, but the angle between the flat tail and the vertical tail should be taken into account, because the incident electromagnetic waves will be reflected multiple times between the flat tail and the vertical tail.

2) Fuselage. The fuselage is the main part of the modeling. The position of the main axis and the shape parameters of the fuselage need to be considered. The shape structure of fuselage, the curve parameters of top, bottom, side and cross section must be considered in the process of modeling.

3) Inlet port. The inlet is a cavity, and its internal structure has a great influence on the scattering. The detailed geometry of the inlet should be taken into account when modeling. The main parameters include the lip curve, the top, bottom, side and cross section curve.

Referring to the parameters of a type of sea-skimming UAV, the model has a wingspan of 7.1 *m*, a fuselage length of 2.6 *m* and a height of 0.87 *m*. The surface material of the model is conventional metal conductor. The model is built in the FEKO software, as shown in Fig. 2. The $\boldsymbol{k_i}$ and $\boldsymbol{k_s}$ are the unit vectors of incident and scattering directions of the radar wave, respectively. θ_i is the incident angle of the radar wave, φ_i is the azimuth angle of the radar wave, θ_s is the scattering angle of the radar wave, φ_s is the azimuth angle of the scattering wave, and γ is the bistatic angle. $\boldsymbol{h_i}$ and $\boldsymbol{v_i}$ are unit vectors of horizontal and vertical polarization directions of incident electromagnetic waves, respectively.

The RCS σ is independent of R when the R is large enough to satisfy the far field condition. R is the distance between radar and UAV. The far field RCS of UAV is:

$$\sigma=\lim_{R\to\infty}4\pi R^2\frac{|\boldsymbol{E}_s|^2}{|\boldsymbol{E}_i|^2}, \quad (9)$$

where $\boldsymbol{E_s}$ is the intensity of scattered electric field and $\boldsymbol{E_i}$

is the intensity of incident electric field. The RCS of the UAV in HH polarization σ_{hh} and VV polarization σ_{vv} are:

$$\sigma_{hh} = \lim_{R\to\infty} 4\pi R^2 \frac{|E_s^h|^2}{|E_i^h|^2}, \quad (10)$$

$$\sigma_{vv} = \lim_{R\to\infty} 4\pi R^2 \frac{|E_s^v|^2}{|E_i^v|^2}, \quad (11)$$

where E_s^h, E_s^v, E_i^h, and E_i^v are the horizontal and vertical polarization components of $\boldsymbol{E}_s$ and $\boldsymbol{E}_i$, respectively.

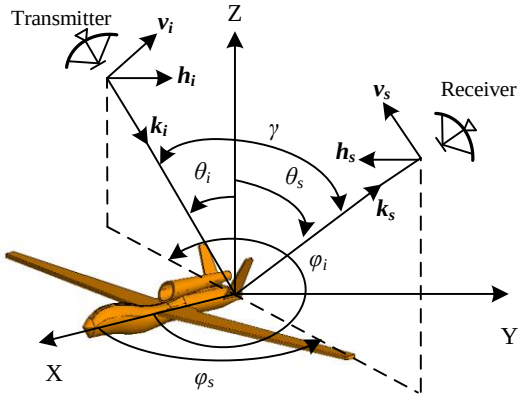

Fig. 2. Simulation model of sea-skimming UAV.

III. RCS ANALYSIS OF SEA-SKIMMING UAV AND ROUGH SEA SURFACE

A. RCS analysis method of rough sea surface

The hardware requirement is high and the computing time is long when the numerical algorithm is used to accurately solve the scattered field of rough sea surface. Accordingly, the PO method based on high frequency approximation is applied to calculate the RCS of rough sea surface quickly. The scattering field of rough sea surface is calculated by the KA method. In the mode of long distance detection of high frequency radar wave, the radius of curvature of rough sea surface is larger than the wavelength and the far field condition is satisfied, so the calculation of scattering field of rough sea surface satisfies the application condition of the PO method.

The PO method uses the induced current on rough sea surface as the source of scattering field, and then integrates the surface current to obtain the scattering field. The scattering field is obtained by integrating the surface current. Figure 3 is a geometric schematic diagram of rough sea surface scattering. The $\boldsymbol{r}'_{\text{sea}}$ is the position vector of scattering source point on rough sea surface and $\boldsymbol{r}_{\text{sea}}$ is the position vector of receiving point. When the plane wave irradiates the rough sea surface, the magnetic vector potential at the receiving point P of the scattered wave is:

$$\boldsymbol{A}_{sea}(\boldsymbol{r}_{sea}) = \frac{\mu_{sea}}{4\pi} \iint_{S_{sea}} \boldsymbol{J}_{sea}(\boldsymbol{r}'_{sea}) \frac{e^{-jkR_{sea}}}{R_{sea}} dS_{sea}, \quad (12)$$

where $\boldsymbol{J}_{sea}(\boldsymbol{r}'_{sea})$ and dS_{sea} are the induced current density and element area at the scattering source point on the sea surface, respectively. μ_{sea} is the sea surface permeability, $\boldsymbol{k}$ is the wave vector, $k = |\boldsymbol{k}| = 2\pi/\lambda$, λ is the wavelength, R_{sea} is the distance from the receiving point to the scattering source point, $\boldsymbol{R}_{sea} = |\boldsymbol{r}_{sea} - \boldsymbol{r}'_{sea}|$.

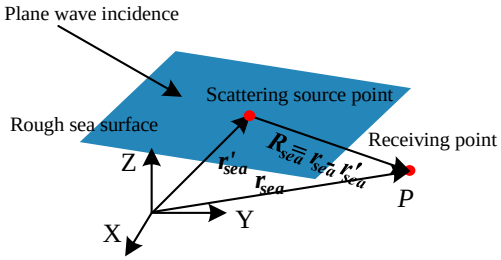

Fig. 3. Geometric schematic diagram of scattering from two-dimensional rough sea surface.

From (12) and far field condition $|k\mathrm{R}|>>1$, the scattering electric field of the sea surface is:

$$\boldsymbol{E}_{sea}(\boldsymbol{r}_{sea}) = \frac{-k^2}{j\omega\varepsilon_{sea}\cdot 2\pi} \iint_{S_L} \boldsymbol{R}_{sea} \times\left[\boldsymbol{R}_{sea}\times(\boldsymbol{n}_{sea}\times\boldsymbol{H}_i)\right]\cdot\frac{e^{-jk\boldsymbol{R}_{sea}}}{R} dS_L, \quad (13)$$

where S_L is the bright area of the scattering object, ε_{sea} is the dielectric constant of the sea surface, and $\boldsymbol{n}_{\text{sea}}$ is the bin normal unit vector of the scattering source point on the rough sea surface.

The expressions of the incident electric field $\boldsymbol{E}_i$ and the incident magnetic field $\boldsymbol{H}_i$ are:

$$\boldsymbol{E}_i(\boldsymbol{r}'_{sea}) = \boldsymbol{E}_0 e^{-j\boldsymbol{k}\boldsymbol{r}'_{sea}}, \quad (14)$$

$$\boldsymbol{H}_i(\boldsymbol{r}'_{sea}) = \frac{1}{\eta}\boldsymbol{k}_0 \times \boldsymbol{E}_i(\boldsymbol{r}'_{sea}), \quad (15)$$

where $\boldsymbol{k}_0$ is the unit vector of the direction of wave vector and η is the wave impedance. The RCS values of rough sea surface can be obtained by substituting (13) and (14) into (15).

B. Optimal method for RCS solution of sea-skimming UAV

Under the incident electric field $\boldsymbol{E}_i$, the scattering electric field generated by surface current of the UAV is as follows:

$$\boldsymbol{E}_{UAV}(\boldsymbol{r}_{UAV}) = -j\omega\boldsymbol{A}_{UAV}(\boldsymbol{r}_{UAV}) - \nabla\phi_{UAV}(\boldsymbol{r}_{UAV}), \quad (16)$$

where j stands for the imaginary symbol, $\boldsymbol{r}_{UAV}$ is the field coordinate vector of receiving point, $\boldsymbol{A}_{UAV}(\boldsymbol{r}_{UAV})$ is the magnetic vector potential of the UAV, and $\phi_{UAV}(\boldsymbol{r}_{UAV})$ is the scalar potential of UAV. $\boldsymbol{A}_{UAV}(\boldsymbol{r}_{UAV})$ and $\phi_{UAV}(\boldsymbol{r}_{UAV})$

are as follows:

$$\boldsymbol{A}_{UAV}(\boldsymbol{r}_{UAV}) = \frac{\mu_{UAV}}{4\pi}\iint_{S_{UAV}} \boldsymbol{J}_{UAV}(\boldsymbol{r}'_{UAV})\frac{e^{-jkR_{UAV}}}{R_{UAV}}dS_{UAV}, \quad (17)$$

$$\phi_{UAV}(\boldsymbol{r}_{UAV}) = \frac{-1}{4\pi j\omega\varepsilon_{UAV}}\iint_{S_{UAV}} \nabla_S \boldsymbol{J}_{UAV}(\boldsymbol{r}'_{UAV}) \cdot\frac{e^{-jkR_{UAV}}}{R_{UAV}}dS_{UAV}, \quad (18)$$

where μ_{UAV} and ε_{UAV} are the permeability and dielectric constant of the UAV conductor, $\boldsymbol{r}'_{UAV}$ is the coordinate vector of scattering source point, $R_{UAV} = |\boldsymbol{r}_{UAV} - \boldsymbol{r}'_{UAV}|$ is the distance from the scattering source point to the receiving point, and $\boldsymbol{J}_{UAV}(\boldsymbol{r}'_{UAV})$ denotes the current density at scattering source point of the UAV surface S_{UAV}, ∇_S is the divergence operator.

It can be seen from (16) that the RCS value of UAV can be obtained by calculating the surface current density. The approximately current distribution of the surface of the UAV can be obtained by the PO method. The difference between the unknown current and the PO current is closer to zero vector. The improvement of computational efficiency can be achieved by using the difference vector instead of the unknown vector.

The conventional MLFMA is an improvement of the MOM, but the initial value of iterative solution of the MLFMA is usually set to zero, which leads to a large gap with the actual target surface current distribution. Therefore, the IMLFMA based on the PO current distribution is proposed to solve the RCS of the UAV in this paper. The iteration times and the computing time are the focus of the proposed algorithm.

The PO surface current density of the UAV expanded by the Rao-Wiltion-Glisson (RWG) basis functions can be expressed as:

$$\boldsymbol{J}_{UAV}(\boldsymbol{r}'_{UAV}) = \frac{1}{2}\boldsymbol{n}_{UAV}\times\boldsymbol{H}_i(\boldsymbol{r}_{UAV}) = \sum_{n=1}^{N_{PO}} a_n f_n(\boldsymbol{r}_{UAV}), \quad (19)$$

where a_n is the scalar coefficient to be calculated and f_n is the basis function of an orthogonal complete set, n = 1, 2,..., N_{PO}. $\boldsymbol{n}_{UAV}$ is the normal unit vector of the surface of the UAV. The coefficient of the basis function can be obtained by:

$$\iint_{S_{UAV}} f_n(\boldsymbol{r}_{UAV})\cdot\frac{1}{2}\boldsymbol{n}_{UAV}\times\boldsymbol{H}_i(\boldsymbol{r}_{UAV})d\boldsymbol{r}_{UAV} = \sum_{n=1}^{N_{PQ}} a_n \iint_{S_{UAV}} f_n(\boldsymbol{r}_{UAV}) f_n(\boldsymbol{r}_{UAV})d\boldsymbol{r}_{UAV}. \quad (20)$$

Assume that the impedance matrix equation is:

$$[Z_{mn}][I_n] = [V_m], \quad (21)$$

where $[Z_{mn}]$ is a general impedance matrix of order $M_{exc}\times N_{PO}$, $[I_n]$ is an unknown matrix of order $N_{PO}\times 1$ and $[V_m]$ is an excitation matrix of order $M_{exc}\times 1$. The elements in the matrix are $I_n = a_n$, Z_{mn} and V_m are inner product of $Z_{mn} = \langle t_m, \boldsymbol{L}(f_n)\rangle$, $V_m = \langle t_m, g_{exc}\rangle$, respectively. Where $\boldsymbol{L}$ stands for a linear operator, g_{exc} denotes an excitation function and t_m (m = 1, 2,..., M_{exc}) is a weight function. For iterative algorithms, the iteration times usually depends on the impedance matrix and the excitation vector. Different excitation vectors $[V_m]$ need different iteration times when the impedance matrix $[Z_{mn}]$ is the same. For the same model, less step is needed to iterate if the surface current is relatively smooth. The iteration times of (21) is zero when there is no incident plane wave. The PO current is used as a correcting current to make $[V_m]$ approach to zero, which can reduce the iteration times and improve the calculation efficiency.

The form of sparse matrix equation (20) is:

$$[Z'_{mn}][I'_0] = [V'_m], \quad (22)$$

where

$$Z'_{mn} = \int_{S_{UAV}} f_m(\boldsymbol{r}_{UAV}) f_n(\boldsymbol{r}_{UAV})d\boldsymbol{r}_{UAV}, \quad (23)$$

$$V'_m = \int_{S_{UAV}} f_m(\boldsymbol{r}_{UAV})\cdot\frac{1}{2}\boldsymbol{n}_{UAV}\times\boldsymbol{H}_i(\boldsymbol{r}_{UAV})d\boldsymbol{r}_{UAV}. \quad (24)$$

The local current vector $[I'_0]$ is extended to the overall current vector $[I_0]$, and the $[I'_0]$ distribution of the original element is retained. Substituting $[I_n - I_0]$ into (21):

$$[Z_{mn}][I_n - I_0] = [V_m] - [Z_{mn}][I_0]. \quad (25)$$

The right part of the equation can be expressed as:

$$[V_0] = [Z_{mn}][I_0]. \quad (26)$$

Replace the initial vector with a zero vector:

$$[Z_{mn}][I_x] = [V_m] - [V_0]. \quad (27)$$

The iterative algorithm is used to solve the matrix equation of (27). After the iterative operation is finished, the calculation result is corrected by $[I_0]$, and the final solution of the electromagnetic scattering problem is:

$$[I_n] = [I_x] + [I_0]. \quad (28)$$

As can be seen from the above process that the PO current matrix is relatively easy to obtain and requires only a small storage space, so the process of solving the impedance matrix equation is also less time consuming. Although another matrix vector multiplication operation is required before the start of the iteration of (27), the total solution time is not significantly increased. After the improvement, the vector $[V_m] - [Z_m]\,[I_0]$ is closer to zero vector than the vector $[V_m]$. Less iterative steps are required during the iterative process to obtain the results of the calculation. Consequently, the IMLFMA based on the PO current can be used to calculate the RCS of UAV quickly and accurately.

C. RCS solution model of sea-skimming UAV and rough sea surface based on FPM

Strict iteration requires too much memory and computing time to solve the coupled electromagnetic scattering between rough sea surface and UAV. The FPM has become one of the most effective models for

solving the coupled scattering field [21]. The FPM has been verified to be able to correctly solve the main electromagnetic scattering between the target object and the sea surface. The FPM can be further simplified using the quasi-mirror method, as shown in Fig. 4.

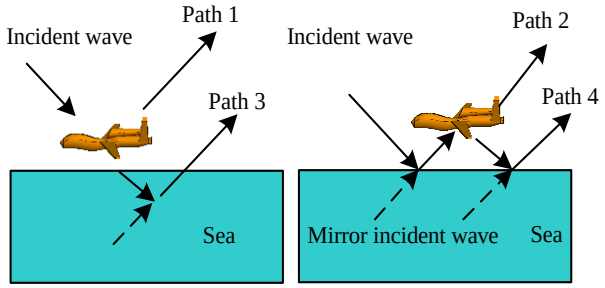

Fig. 4. Simplified four-path model.

According to the idea of the FPM, the composite scattering of rough sea surface and UAV includes the scattering electric field $\boldsymbol{E}_{UAV}$ of the UAV, the scattering electric field $\boldsymbol{E}_{sea}$ of the sea surface and the coupling scattering $\boldsymbol{E}_{co}$ between the sea surface and the UAV. The composite RCS σ_c of rough sea surface and UAV can be obtained by the hybrid algorithm of the PO method and the IMLFMA (PO-IMLFMA) based on the FPM, as shown in the following formula:

$$\sigma_c = 4\pi \lim_{R\to\infty} R^2 \left|\boldsymbol{E}_{UAV} + \boldsymbol{E}_{sea} + \boldsymbol{E}_{co}\right|^2 \Big/ \left|\boldsymbol{E}_i\right|^2 , \quad (29)$$

where R is the distance from the receiving point to the scattering source point. $\boldsymbol{E}_{UAV}$ is obtained by the IMLFMA. $\boldsymbol{E}_{sea}$ is obtained by the PO method. It can be seen from Fig. 4 that the coupled scattering field contains the scattering contribution of the path 2 - 4. The coupling scattering between the sea surface and the UAV is:

$$\boldsymbol{E}_{co} = \boldsymbol{E}_{os}^{second} + \boldsymbol{E}_{so}^{second} + \boldsymbol{E}_{sos}^{third} , \quad (30)$$

where $\boldsymbol{E}_{os}^{second}$ is the secondary coupling scattering of "UAV-Sea Surface". $\boldsymbol{E}_{so}^{second}$ is the secondary coupling scattering of "Sea Surface-UAV". $\boldsymbol{E}_{sos}^{third}$ is the third coupling scattering of "Sea Surface-UAV-Sea Surface". As shown in Fig. 4, combined with the quasi-mirror method, the coupling scattering calculation between UAV and sea surface can be further simplified by using the mirror radar and mirror UAV instead of the reflection of rough sea surface. A correlation reflection coefficient $\boldsymbol{E}_{co}$ is defined to simulate the reflection of sea rough surface in the calculation:

$$\boldsymbol{E}_{co} = r\boldsymbol{E}_{UAV}^{i\text{-}s'} + r\boldsymbol{E}_{UAV}^{i'\text{-}s} + r^2\boldsymbol{E}_{UAV}^{i'\text{-}s'} , \quad (31)$$

where r is the position of the receiving point. $\boldsymbol{E}_{UAV}$ is the scattering electric field of the UAV, the superscripts $\boldsymbol{i}'$ and $\boldsymbol{s}'$ are the mirror directions of the incident direction $\boldsymbol{i}$ and scattering direction $\boldsymbol{s}$, respectively.

IV. RCS COMPENSATION METHOD FOR SEA-SKIMMING UAV BASED ON BP NEURAL NETWORK

In practice, the RCS value of UAV that is not affected by any interference is what we really need. However, the RCS of sea-skimming UAV is seriously affected by the sea conditions. The RCS values measured directly cannot accurately reflect the actual situation of UAV. Therefore, a RCS compensation model of sea-skimming UAV based on BP neural network is presented in this paper. The relationship between the input factors and the RCS values of sea-skimming UAV can be mapped by BP neural network as shown in Fig. 5.

In actual RCS measurements, it is easy to obtain the direction of incident wave, the azimuth angle, the RCS value of sea surface and the composite RCS value of target object and sea surface. Therefore, the input factors $\boldsymbol{X}$ are expressed by:

$$\boldsymbol{X} = (\theta_i, \varphi_i, \sigma_{sea}, \sigma_c)^{\mathrm{T}} , \quad (32)$$

where θ_i (°) represents the incident angle, φ_i (°) represents the azimuth angle of airborne detection radar, σ_{sea} (dBsm) represents the monostatic RCS value of sea surface and σ_c (dBsm) stands for composite monostatic RCS value of sea surface and UAV. The number of neurons in the input layer is 4. The output factor $\boldsymbol{Y}$ is represented by:

$$\boldsymbol{Y} = \sigma_{UAV} , \quad (33)$$

where σ_{UAV} (dBsm) represents monostatic RCS value of sea-skimming UAV. The number of neurons in the output layer is 1. The number of neurons in the hidden layer is an empirical range integral value h affected by the number of neurons in the input and output layers. The detailed calculation of h is:

$$h = \sqrt{5} + c , \quad (34)$$

where c denotes a constant in the interval [0,10], which the specific value depends on the actual situation.

The BP neural network of sea-skimming UAV is a small and middle neural network, so one hidden layer is adopted. The transfer function of the hidden layer is set to the sigmoid function. The output layer transfer function of the BP neural network of the sea-skimming UAV is taken as a linear function. In the process of forward propagation of BP neural network, the information is transmitted from the input layer to the output layer and processed by each layer. The output of the neural network is:

$$y_1 = \sum_{j=1}^{h} \frac{v_{j1}}{\exp\left[-\sum_{i=1}^{4}\left(\omega_{ij}x_i + \theta_j\right)\right] + 1} + b_1 , \quad (35)$$

where w_{ij} is the weight between the i-th neuron of the input layer and the j-th neuron of the hidden layer, and v_{jk} is the weight between the j-th neuron of the hidden layer and the k-th neuron of the output layer, θ_j is the

threshold of the *j*-th neuron in the hidden layer, and b_1 is the threshold of the output layer neuron.

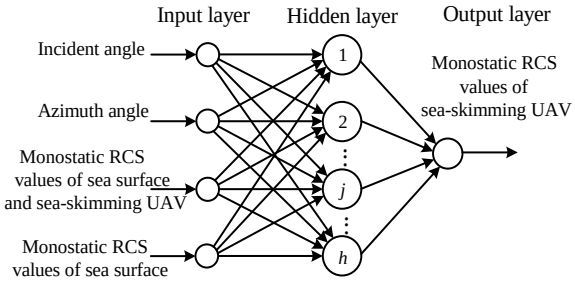

Fig. 5. Topological structure of RCS compensation model for sea- skimming UAV based on BP neural network.

When the results of output layer do not meet the requirements of the target, the information is transferred to the backpropagation state, and the error signal is returned back along the original path. In this process, the weights of the neurons in each layer will be modified sequentially, and the error signal can meet the mean square error accuracy requirement through repeated iterations.

The weights and thresholds of the hidden layer and the output layer are adjusted in a similar way, taking the output layer as an example here. Assuming that there are *n* training samples, and the mean square error of the *i*-th training sample is:

$$e=\frac{1}{2}\left(\sigma_{UAV0}^{i}-\sigma_{UAV}^{i}\right)^{2}, \tag{36}$$

where σ_{UAV0}^{i} and σ_{UAV}^{i} are the exact and actual output values of the neuron for the *i*-th RCS sample, respectively. The weights and thresholds of each layer are adjusted by the Levenberg-Marquardt (L-M) algorithm. The specific adjustment way of weights is:

$$w_{k+1}=w_k+\Delta w_k, \tag{37}$$

$$\Delta w_k=-\left[J^T(w_k)J(w_k)+\mu I\right]^{-1}J^T(w_k)\cdot e, \tag{38}$$

where w_k and w_{k+1} are the weights before and after the adjustment of each layer. *J* is a Jacobi matrix of the error *e* with respect to the weight *w*. μ is a scalar factor, and *I* is an identity matrix. The L-M algorithm controls the iteration speed by changing the value of μ in the iteration process of the sea-skimming UAV neural network, so as to ensure that the calculation speed can be improved under the condition that the accuracy requirement is met.

The neural network stops training and outputs weights and thresholds when the global error *E* of the trained network satisfies the target requirement or the training iteration number reaches the maximum iteration number. The global error *E* can be expressed as:

$$E=\frac{1}{2n}\sum_{i=1}^{n}\left(\sigma_{UAV0}^{i}-\sigma_{UAV}^{i}\right)^{2}. \tag{39}$$

V. VERIFICATION AND ANALYSIS

The centimeter wave radar is often used to detect targets in the maritime and aerial field, so the calculation frequency is generally set above 2 GHz. In this paper, the incident frequency is set to 3 GHz, and the corresponding wavelength λ = 0.1 *m*. The electric size of the UAV is about 71 λ. This type of sea-skimming UAV is an electrically large size object. The excitation source is approximately plane wave. The azimuth angle of scattering wave is 0° at the head, and 180° at the tail of the UAV.

The composite RCS calculation model is obtained by combining the sea surface model and the sea-skimming UAV model in different sea conditions, as shown in Fig. 6. The reference model of the sea surface is located in the XOY plane, and the relative dielectric constant of seawater is 81.5. The size of sea surface is 500 λ × 500 λ.

This paper mainly studies an extremely low flying UAV over the very large size sea surface. The small range of variation of the flying height of the sea-skimming UAV has a weak influence on the coupling scattering, so the influence of a small range of variation in the flight height can be neglected. The vertical height *h* of the center point of the UAV from the sea surface is set to 15 *m*.

A. Verification of RCS solution method for UAV and rough sea surface

In order to verify the solving accuracy, the operation efficiency and hardware memory requirements of the PO-IMLFMA method based on the FPM for the composite RCS of rough sea surface and sea-skimming UAV, this paper uses the PO-MOM method based on the FPM and the conventional MLFMA as contrast methods to solve and analyze the RCS of composite model. When using the PO-IMLFMA method, the RCS of sea surface is solved by the PO method and the RCS of UAV is solved by the IMLFMA. Similarly, the RCS of sea surface and UAV are solved respectively by the PO method and the MOM when using the PO-MOM algorithm. The MLFMA is an accurate method, which can provide high accuracy for solving RCS values [22]. The incident angle θ_i is 40° and the azimuth angle φ_i of incident wave is 90°, the scattering azimuth angle φ_s is 90°, and the scattering angle θ_s ranges from [-90°, 90°].

The calculation results of the composite bistatic RCS of sea surface and sea-skimming UAV solved by three algorithms are shown in Fig. 7. The RCS calculation results of the three algorithms under the VV polarization and HH polarization are generally

consistent. The calculation results of the PO-IMLFMA method based on the FPM and the PO-MOM method based on the FPM are close, and the RCS values at some scattering angles are smaller than those of the conventional MLFMA, because the model of rough sea surface is solved approximately by the PO algorithm. The accuracy of the hybrid algorithm is limited in calculating the scattering field of some angles, but the error is small, and does not affect the overall composite RCS analysis.

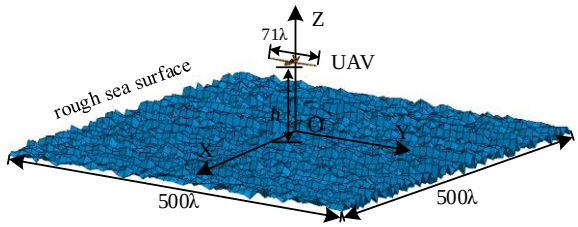

Fig. 6. Composite RCS calculation model of rough sea surface and sea-skimming UAV.

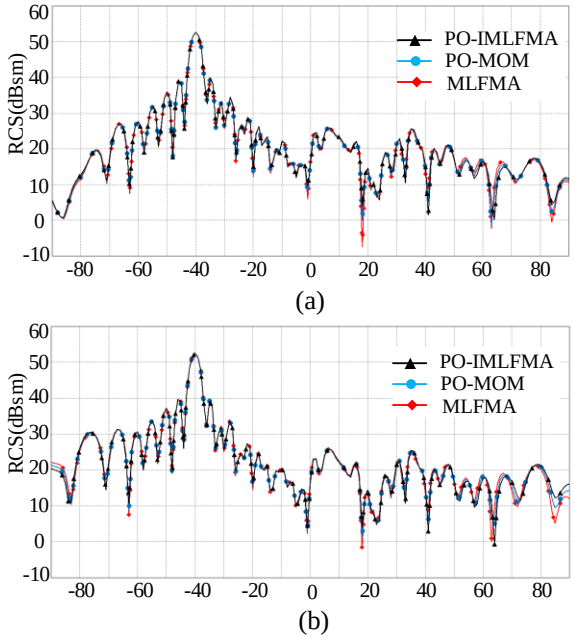

Fig. 7. Comparison of the bistatic RCS results for the composite model of rough sea surface and sea-skimming UAV calculated by different methods. (a) VV polarization. (b) HH polarization.

Table 2: Comparison between PO-IMLFMA, PO-MOM and MLFMA method (VV Polarization)

Method	Memory (MB)	Computing Time (s)
PO-IMLFMA	295	768
PO-MOM	751	2963
MLFMA	1765	5687

The memory requirement and computing time of the three methods in the VV polarization are compared as shown in Table 2. It is obvious from the data in the table that the memory required by the two hybrid algorithms is much less than that of the MLFMA, and the computational efficiency is much higher than the MLFMA. Compared with the PO-MOM method, the PO-IMLFMA method saves more memory space and less computation time. This is due to the fact that the memory consumption and computational complexity of the IMLFMA are lower than those of the MOM when calculating the composite model RCS for UAV area alone, which leads to lower memory consumption and higher computational efficiency when using the PO-IMLFMA hybrid algorithm. The results verify that the hybrid algorithm of the PO-IMLFMA method based on FPM can effectively and efficiently analyze the composite RCS of sea-skimming UAV under different sea conditions.

B. RCS compensation of sea-skimming UAV under different sea conditions

The RCS compensation model topology of sea-skimming UAV in Fig. 5 is adopted. In order to ensure the generality of training samples and combine the actual situation of monostatic RCS of sea-skimming UAV, the range of incident angle θ_i is [10°,80°], and the interval is 10°, the range of azimuth angle φ_i is [0,360°], and the interval is 5°. The composite monostatic RCS samples σ_c of BP neural network are obtained by PO-IMLFMA method proposed above. The monostatic RCS value σ_{sea} of sea surface and the monostatic RCS value σ_{UAV} of UAV are calculated by the PO method and the IMLFMA, respectively. The detailed relationships are shown in Fig. 8. The number of training samples under the 1-scale, 3-scale and 5-scale sea conditions is 1752 (3×8×73) groups. The maximum number of iterations is set to 100. The data of some training samples is shown in Table 3. The number of the hidden layer h is 9. The RCS compensation model of sea-skimming UAV based on BP neural network can be obtained after training the sample data of sea-skimming UAV.

On the platform of VV polarized airborne radar, the RCS compensation model of sea-skimming UAV based on BP neural network is used to compensate the monostatic RCS under the 1-scale, 3-scale and 5-scale sea conditions. To verify the validity of the compensation model, the incident angle and azimuth angle data of the selected test samples are different from the training samples. The incident angles are 65°, 45° and 25°. The range of azimuth angle is [0,360°], and the interval is 1°. The RCS compensation results of sea-skimming UAV under the 1-scale, 3-scale and 5-scale sea conditions are shown in Fig. 9, Fig. 10 and Fig. 11, respectively. The uncompensated result stands for the monostatic RCS values of the sea-skimming UAV affected by sea

conditions. The expected value stand for the RCS of sea-skimming UAV under the same detection conditions. The compensated result stand for the monostatic RCS of sea-skimming UAV generated by the compensation network. It can be seen from Figs. 9-11 that the overlap ratio of compensation results and the expected values of different sea conditions is higher when the incident angle is 65° and 45°. However, the overlap ratio of curves decreases obviously when the incident angle is 25°. This is due to the fact that the detection radius of UAV detected by airborne radar at low incident angle is small at the same altitude, and the variation of RCS with the azimuth angle is not obvious. The smaller the incident angle is, the closer the detection direction is to vertical overlooking, and the contribution of sea surface scattering is stronger. The scattering characteristics of UAV are almost completely covered up by the sea surface when the incident angle is small.

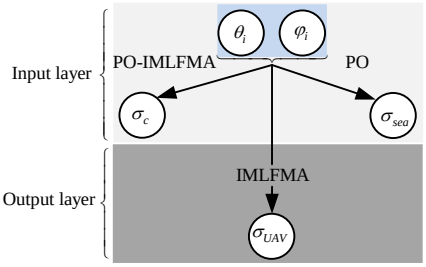

Fig. 8. Relation diagram of training samples and its solution algorithms.

Table 3: Part of the training samples

Number	θi (°)	φ_i (°)	σ_c (dBsm)	σ_{sea} (dBsm)	σ_{UAV} (dBsm)
1	10	0	24.59	19.88	19.06
2	10	0	19.69	18.32	19.06
3	10	0	28.25	26.18	19.06
4	10	5	23.22	17.52	9.75
5	10	10	15.16	13.73	10.29
6	10	15	12.33	14.67	2.17
7	10	20	21.16	18.50	-1.17
8	20	0	30.48	28.15	-8.99
9	30	0	18.27	-1.50	-0.27
10	40	0	20.25	20.01	-6.33
11	50	0	19.36	18.21	-3.79
12	60	0	13.47	14.90	0.37

The mean values of the three cases are shown in Table 4. The compensation error under the 1-scale sea condition is less than 0.95 dBsm, under the 3-scale sea condition is less than 0.41 dBsm, and under the 5-scale sea condition is less than 1.94 dBsm. The compensation error denotes the difference between expected value and compensated value. Compared with the uncompensated value, the mean error of the compensated result is smaller, which verifies the effectiveness of the RCS compensation scheme of the sea-skimming UAV based on BP neural network.

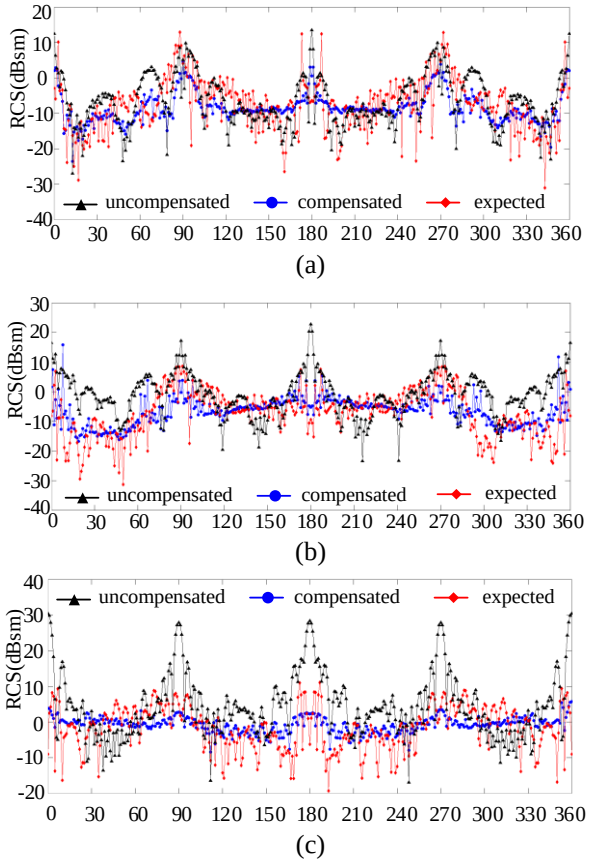

Fig. 9. Monostatic RCS compensation results of sea-skimming UAV under 1-scale sea condition. (a) Incident angle 65°. (b) Incident angle 45°. (c) Incident angle 25°.

The BP neural network compensation model can significantly reduce the impact of sea conditions on the overall RCS of the sea-skimming UAV, but it is difficult to accurately obtain the scattering characteristics of the sea-skimming UAV with the azimuth variation. Actually, the general airborne radar is far away from the sea-skimming UAV, and the radar wave has a large incident angle. Therefore, the compensation model can be employed to most cases, and the error after compensation is insignificant, which can effectively obtain the RCS indicating the electromagnetic scattering characteristics of sea-skimming UAV.

In the actual environment, the RCS value of the UAV can be obtained by compensation algorithm, which can help the relevant personnel directly and effectively analyze the detected characteristics of the flying object, such as aircraft type. This compensation algorithm has a broader application space in the field of military anti-reconnaissance.

Table 4: RCS compensation result of sea-skimming UAV considering sea conditions

Scale	Angle	Uncompensated (dBsm)	Compensated (dBsm)	Expected (dBsm)	Error (dBsm)
1	65°	-6.51	-8.45	-7.50	0.95
	45°	-0.94	-6.51	-7.14	-0.63
	25°	4.15	-0.85	-1.53	-0.68
3	65°	17.71	-7.91	-7.50	0.41
	45°	19.54	-6.74	-7.14	-0.4
	25°	20.84	-1.13	-1.53	-0.4
5	65°	10.81	-8.71	-7.50	1.21
	45°	15.07	-7.06	-7.14	-0.08
	25°	19.50	-3.47	-1.53	1.94

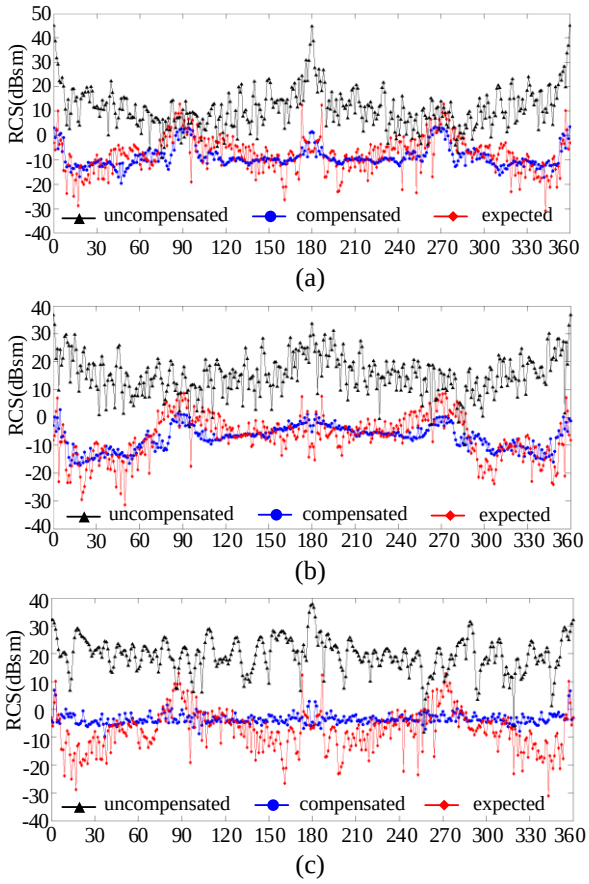

Fig. 10. Monostatic RCS compensation results of sea-skimming UAV under 3-scale sea condition. (a) Incident angle 65°. (b) Incident angle 45°. (c) Incident angle 25°.

VI. CONCLUSION

The far field RCS of the sea-skimming UAV and rough sea surface is studied in this paper. A rough sea surface model is established by using the PM spectrum and Monte Carlo method, and a fast algorithm for the sea surface RCS based on the PO method is applied. Then, a composite model of rough sea surface and the sea-skimming UAV is established, and a hybrid algorithm of the PO-IMLFMA method based on the application of PO method and IMLFMA method for solving the RCS of the composite model based on the FPM is proposed. Compared with the IMLFMA and the PO-MOM, the PO-IMLFMA has the advantages of less memory consumption (about 295 MB) and faster solution speed (about 768 s) for solving the composite model.

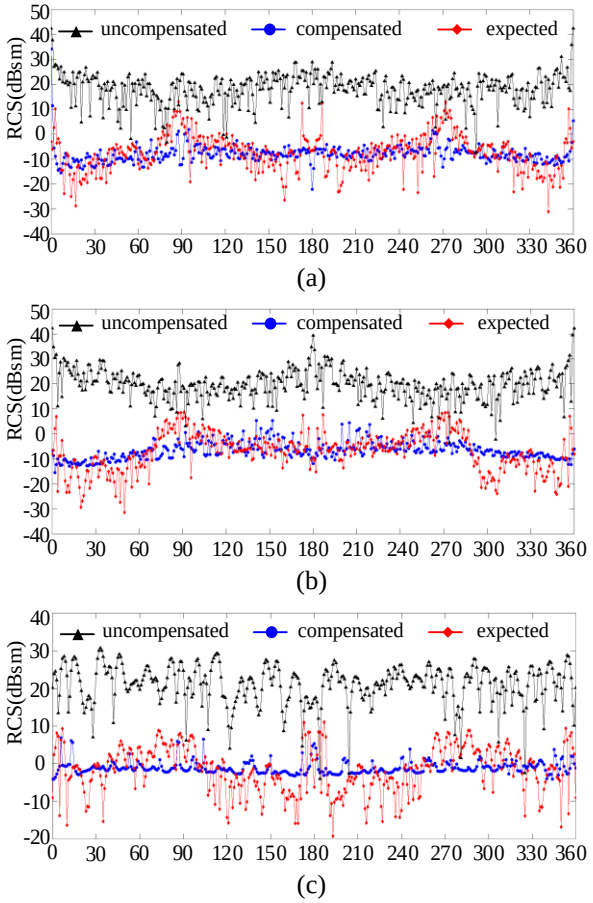

Fig. 11. Monostatic RCS compensation results of sea-skimming UAV under 5-scale condition. (a) Incident angle 65°. (b) Incident angle 45°. (c) Incident angle 25°.

In addition, in view of the influence of rough sea surface on the RCS values of UAV, the RCS compensation scheme of UAV based on BP neural network is proposed. Moreover, the efficiency of BP neural network compensation scheme is verified by an example analysis. The compensation results demonstrate that the compensation errors under the 1-scale, 3-scale and 5-scale sea conditions are less than 0.95 dBsm, 0.41 dBsm and 1.94 dBsm respectively, namely the compensation scheme significantly reduces the influence of sea conditions.

REFERENCES

[1] Y. Fu, M. Ding, C. Zhou, and H. Hu, "Route planning for unmanned aerial vehicle (UAV) on the sea using hybrid differential evolution and quantum-behaved particle swarm optimization," *IEEE Trans. Syst. Man Cybern. Syst*., vol. 43, no. 6, pp. 1451-1465, Nov. 2013.

[2] Y. Zhao, M. Zhang, H. Chen, and X. Yuan, "Radar scattering from the composite ship-ocean scene: Doppler spectrum analysis based on the motion of six degrees of freedom," *IEEE Trans. Antennas Propag*., vol. 62, no. 8, pp. 4341-4347, Aug. 2014.

[3] A. V. Khristenko, et al., "Magnitude and spectrum of electromagnetic wave scattered by small quad-copter in X-band," *IEEE Trans. Antennas Propagat*., vol. 66, no. 4, pp. 1977-1984, Apr. 2018.

[4] M. Pieraccini, L. Miccinesi, and N. Rojhani, "RCS measurements and ISAR images of small UAVs," *IEEE Aero. El. Syst. Mag*., vol. 32, no. 9, pp. 28-32, Sep. 2017.

[5] A. V. Khristenko, et al., "Magnitude and spectrum of electromagnetic wave scattered by small quad-copter in X-band," *IEEE Trans. Antennas Propagat*., vol. 66, no. 4, pp. 1977-1984, Apr. 2018.

[6] M. Pieraccini, L. Miccinesi, and N. Rojhani, "RCS measurements and ISAR images of small UAVs," *IEEE Aero. El. Syst. Mag.*, vol. 32, no. 9, pp. 28-32, Sep. 2017.

[7] G. Çakir, M. Çakir, and L. Sevgi, "An FDTD-based parallel virtual tool for RCS calculations of complex targets," *IEEE Antennas Propagat. Mag*., vol. 56, no. 5, pp. 74-90, Oct. 2014.

[8] A. Sefer, M. A. Uslu, and L. Sevgi, "MATLAB-based 3-D MoM and FDTD codes for the RCS analysis of realistic objects [Testing Ourselves]," *IEEE Antennas Propagat. Mag*., vol. 57, no. 4, pp. 122-148, Aug. 2015.

[9] L. Zhang, N. Yuan, M. Zhang, L. Li, and Y. Gan, "RCS computation for a large array of waveguide slots with finite wall thickness using the MoM accelerated by P-FFT algorithm," *IEEE Trans. Antennas Propag.*, vol. 53, no. 9, pp. 3101-3105, Sep. 2005.

[10] J. Lee, J. Zhang, and C.-C. Lu, "Sparse inverse preconditioning of multilevel fast multipole algorithm for hybrid Integral equations in electro-magnetics," *IEEE Trans. Antennas Propag*., vol. 52, no. 9, pp. 2277-2287, Sep. 2004.

[11] Ö. Ergul and L. Gurel, "Efficient parallelization of the multilevel fast multipole algorithm for the solution of large-scale scattering problems," *IEEE Trans. Antennas Propag*., vol. 56, no. 8, pp. 2335-2345, Aug. 2008.

[12] F. T. Ulaby and C. Elachi, *Radar Polarimetry for Geoscience Application*. Boston, MA, USA: Artech House, 1990.

[13] J. A. Ogilvy, *Theory of Wave Scattering From Random Rough Surfaces*. Bristol, U.K.: Inst. of Physics, 1991.

[14] C. Corbel, C. Bourlier, N. Pinel, and J. Chauveau, "Rough surface RCS measurements and simulations using the physical optics approximation," *IEEE Trans. Antennas Propag*., vol. 61, no. 10, pp. 5155-5165, Oct. 2013.

[15] W. J. Pierson, Jr. and L. Moskowitz, "A proposed spectral form for fully developed wind seas based on the similarity theory of S. A. Kitaigorodskii," *J. Geophys. Res*., vol. 69, no. 24, pp. 5181-5190, Jan. 1964.

[16] T. Elfouhaily, B. Chapron, K. Katsaros, and D. Vandemark, "A unified directional spectrum for long and short wind-driven waves," *J. Geophys. Res.*, vol. 102, no. C7, pp. 15781-15796, Feb. 1997.

[17] O. M. Phillips, "The equilibrium range in the spectrum of windgenerated waves," *J. Fluid Mech*., vol. 4, no. 4, pp. 426-434, Aug. 1958.

[18] J. W. S. Rayleigh, *The Theory of Sound*. Macmillan, London, 1877.

[19] M. R. Pino, R. J. Burkholder, and F. Obelleiro, "Spectral acceleration of the generalized forward-backward method," *IEEE Trans. Antennas Propag*., vol. 50, no. 6, pp. 785-797, June 2002.

[20] B. Hu and W. C. Chew, "Fast inhomogeneous plane wave algorithm for scattering from objects above the multilayered medium," *IEEE Trans. Geosci. Remote Sens*., vol. 39, no. 5, pp. 1028-1038, May 2001.

[21] T. Rashid, *Make Your Own Neural Network, Charleston*. Create Space Independent Publishing Platform, Charleston, 2016.

[22] M. Hassoun, *Fundamentals of Artificial Neural Networks*. Bradford Book, Cambridge, 2003.